ISSN: 2664-9640

Based on the critical state of CO_2 under different nozzles Flow field characteristic analysis

Na Liu[1], Guangzhong Hu[1], Tao Lu [1], Yingbiao Wang [2], Anlin Hu [2]

[1] School of mechanical engineering, light chemical industry in Sichuan University, Sichuan 644000, China;

[2]Weitelong Fire Safety Group Co., Ltd, Chengdu 610000, China;

595546316@qq.com, hgzdhx@163.com

Abstract

Aiming at the influence of the decompression phase change behavior of the critical state CO_2 in the nozzle on its jet performance, straight tube nozzles, tapered tube nozzles, shrinking tube nozzles, expanding tube nozzles, and Laval nozzles are the research objects. Through the establishment of a 2000mm×600mm external flow field, when the inlet pressure is 5MPa, the inlet temperature is 285.15K, the outlet pressure is atmospheric pressure, and the outlet temperature is 300K, it is constructed using Fluent's evaporation and condensation model and user-defined UDF functions. CO_2 three-phase conversion model, combined with Realizable k-ε turbulence model and VOF multiphase flow model, established five finite element simulation models of nozzles. The research results show that: 1) Dry ice is formed at the outlet of each nozzle and continuously sublimates and dissipates along the jet direction. Dry ice can only stay in a short time and a short distance, and there is no ice blockage inside the nozzle. 2) Among the five types of nozzles, the expansion nozzle has the best jet effect. Its energy loss is small along the jet direction, the speed is maintained at 107m/s, and its gasification degree reaches 75% at the end of the flow field, and the jet coverage is the largest. Therefore, the use of pipe expansion nozzles will be more conducive to extinguishing fires.

Keywords

Nozzle; Fluent; CO2;UDF.

1. Introduction

According to statistics, large-scale oil storage tanks at home and abroad have frequent fire accidents caused by fires in sealing rings and fire dikes. 2019 national reports 233000 fire, death of 1335 people, injured 837 people, direct property loss 3.6 billion yuan. At present, large-scale storage tanks mainly use foam fire extinguishing systems, but this system has problems such as inappropriate foam mixing ratio, slow start-up speed, secondary pollution, and corrosion [1]. As a clean, effective, cheap and easy-to-obtain fire extinguishing agent, CO_2 has been widely used in many fire protection fields such as ships, mines, and cultural relics protection, but it is rarely used in large oil storage tank fires. Woolley et al [2-3] used the CO_2 spherical tank discharge experiment and concluded that a highly under-expanded jet will be generated near the leak of the CO_2 pipeline, and dry ice will be generated during the jet. Huh et al. [4] found through experiments and simulations that the sudden expansion of the volume of CO_2 caused by gasification during venting caused a sharp drop in pressure and temperature, and the greater the initial pressure drop when it was closer to the leak. Witlox et al [5-6] found through high-pressure liquid phase CO_2 and high-pressure supercritical CO_2 release experiments that the solid CO_2 produced will quickly volatilize and will not cause a

ISSN: 2664-9640

sedimentation process. Proust[7] et al found through dense phase CO_2 leakage and diffusion experiments that, due to the extremely fast condensation rate, the dry ice particles generated in the near-field expansion zone of the discharge are extremely small, and because of sublimation, no dry ice sedimentation is seen in the far-field diffusion zone. , This experiment cannot predict the dry ice score. Dnv G L[8] studied the rapid decompression behavior of high-pressure liquid CO_2 and the phase transition process and found that the phase transition rate determines its superheat and release of heat. Lowest temperature of the nozzle, and the heat treatment had no direct effect on pressure and temperature. Ahmad et al [9] conducted large-scale, full-caliber, dense phase CO_2 buried pipeline fracture experiments and found that the Storage tanks minimum temperature of -17.8 ℃, tube the lowest temperature is -78 ℃. At present, a large number of studies have been conducted on the characteristics of high-pressure CO_2 jets, but there are very few studies based on the performance of CO_2 jets near the gas-liquid saturation line. Therefore, this paper uses the Fluent evaporation and condensation model combined with user-defined UDF functions to determine the CO_2 storage pressure at 5MPa and Simulating the pressure relief jet process under different nozzles at 285.15K, by simulating the process of different kinds of nozzle jet, Analysis inside the nozzle and the flow field in the change law of carbon on critical CO2 in large oil tank fire prevention and extinguishing has important guiding significance.

2. Phase transition model establishment

The triple point and critical point in the CO_2 phase diagram (Figure 1-1) do not exist in theory, and their corresponding values are approximate reference values measured through countless experiments. Under a certain stable pressure and temperature, CO_2 gas will present a state of equilibrium in which the gas phase and the liquid phase coexist, forming a saturated vapor curve, or BC line, on which the corresponding pressure value is the saturated vapor pressure. In the same way, there is a sublimation curve formed by the gas phase and the solid phase in equilibrium, namely the A B line, and the melting curve formed by the liquid phase and the solid phase in the equilibrium state, namely the line BD. CO2 with the change of pressure, temperature, showing gaseous, liquid, solid, supercritical Four phase, and physical properties such as density, viscosity, a great change of the invasive; CO_2 in each phase range is extremely susceptible The change of temperature and pressure causes the transformation between phases. When the temperature of CO_2 is higher than the triple point temperature, when the pressure rises and crosses the gas-liquid saturation line BC, the state of CO_2 will change from gas to liquid; conversely, when the temperature of CO_2 is lower than the three-phase In the case of low temperature, when the pressure rises and crosses the gas-solid saturation line AB, CO_2 will transform from gas to solid to form dry ice; When air pressure is 0.1 Mpa, the equilibrium point of gas-solid two phases is -78.5 ℃, as the temperature increases, dry ice will directly sublimate into gaseous CO_2.

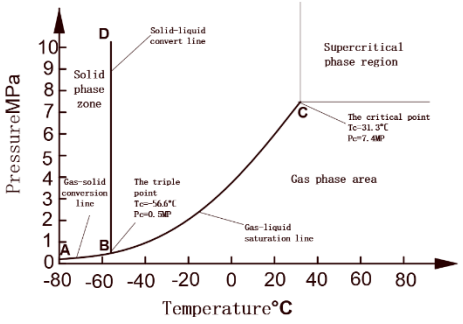

Figure.1 Carbon phase diagram[]

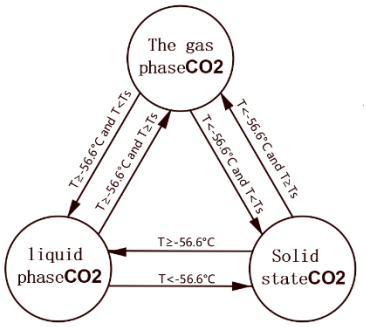

Figure.2 CO_2 phase state conversion diagram

ISSN: 2664-9640

After the CO_2 jet starts, the fluid medium will undergo a decompression phase change, rapidly forming a multiphase flow and propagating in the nozzle with the decompression wave, and finally ejected into the atmosphere in the form of a highly under-expanded jet. Decompression phase transition is divided into two aspects: time scale and temperature change, and can be divided into two types: equilibrium thermodynamic state and non-equilibrium thermodynamic state. Equilibrium thermodynamics state refers to the cavitation flow in a relatively small time scale and temperature change, and the temperature is at a low state; non-equilibrium thermodynamics state refers to the violent generation of thermal fluid under the decompression effect (i.e., the Joule Thomson effect) The phase change and relatively strong mass and heat transfer can be regarded as the boiling phenomenon that is caused by the pressure drop, that is, flash evaporation; therefore, the CO_2 jet should be regarded as a non-equilibrium thermal state caused by the reduced pressure phase change. From the CO_2 phase diagram, it can be seen that when the pressure is below 10MPa, the melting curve BD can be regarded as a vertical line with a temperature of -56.6℃. The complex phase transition between phases is transformed into a flashing phase transition model formed by gas-liquid two phases. According to the physical property changes corresponding to the CO_2 jet flash evaporation process, it is combined with the multiphase flow model, and its decompression phase change model is established through the evaporation and condensation model in the FLUENT software. In the evaporation and condensation process, in order to enable the solver in Fluent to dynamically capture the saturation temperature value corresponding to the pressure of the medium at different times, so that the solver in Fluent can calculate the mass source term and energy source term. Therefore, the user need to build mass transfer model in Fluent carbon dioxide under the different pressure of saturated temperature curve, namely the saturation temperature corresponding to the pressure function.

The fitting polynomial formula of the gas-liquid saturation line BC is (0.5186MPa≦P≦7.4MPa):

$$\begin{aligned} T_{sat1} &= 193.00567 + 54.70812*10^{-6}*P - 18.62179*10^{-12}*P^2 \\ &+4.07283*10^{-18}*P^3 - 0.4556*10^{-24}*P^4 + 0.01994*10^{-30}*P^5 \end{aligned} \quad (1)$$

Formula: p at any time for the unit area of the pressure in the flow field numerical,Pa; T is the saturation temperature corresponding to the unit area at any time, K.The saturated vapor pressure formula on the gas-solid saturation is line AC (0MPa≦P<0.5186MPa):

$$P_S = 9.44*10^5 \exp(-\frac{3108.2}{T_w}) \quad (2)$$

Formula: P_S is the saturated vapor pressure, Mpa; TW is the temperature, K.

The corresponding formula for saturation temperature is derived from the above Formula as:

$$T_{sat2} = -3108.2 \div \ln(P \div (9.44*10^{11})) \quad (3)$$

Formula: p at any time for the unit area of the pressure in the flow field numerical, Pa; Tsat2 is the saturation temperature corresponding to the unit area at any time, K.

The equation of FLUENT evaporation and condensation is as follows:

(1) Evaporation process $T_L > T_{sat}$

Gas phase quality source term

$$S_M = A*\alpha_L*\rho_L*\left|\frac{T_L - T_{sat}}{T_{sat}}\right| \quad (4)$$

Liquid phase quality source term

$$S_M = -A*\alpha_L*\rho_L*\left|\frac{T_L - T_{sat}}{T_{sat}}\right| \quad (5)$$

ISSN: 2664-9640

Energy source term

$$S_M = -A * \alpha_L * \rho_L * \left| \frac{T_L - T_{sat}}{T_{sat}} \right| \Delta H \tag{6}$$

Condensation process $T_L < T_{sat}$

Gas phase quality source term

$$S_M = -B * \alpha_V * \rho_V * \left| \frac{T_V - T_{sat}}{T_{sat}} \right| \tag{7}$$

Liquid phase quality source term

$$S_M = B * \alpha_V * \rho_V * \left| \frac{T_V - T_{sat}}{T_{sat}} \right| \tag{8}$$

Energy source term

$$S_M = B * \alpha_V * \rho_V * \left| \frac{T_V - T_{sat}}{T_{sat}} \right| \Delta H \tag{9}$$

Formula: T_L , T_V is the temperature of the liquid and gaseous medium respectively, K ; T_{sat} is the saturation temperature of the medium at the specified pressure, K ; ΔH heat of vaporization corresponding to the saturation temperature at the specified pressure J / Kg ; α_L and α_V is the volume of the liquid and gaseous media respectively Fraction; ρ_L and α_L is the density of the liquid and gaseous medium respectively, kg / m^3 ; S_M are the mass source terms $kg/(m^2 \cdot s)$ corresponding to the medium, A and B as the coefficient of mass transfer rate, should be adjusted according to the nozzle model, the larger the A, B, the hours, the higher the degree of gasification, the bigger the mass transfer of liquid to gas phase, the lower nozzle temperature;A ,B, ΔH have significant effects on medium energy source term.

3. Physics and Mathematical Model

3.1. Nozzle geometry model

The nozzle is a key component of the entire spray system, and the rationality of its structural design has a significant impact on the overall spray performance. The nozzle should try to convert the pressure energy of the jet fluid into effective kinetic energy, and the head loss and stream entrainment should be as small as possible, and the jet fluid should be kept stable without clogging.

Straight nozzle [9] (Figure a) is easy to process and meets the general jet performance requirements, but the flow channel resistance is large, the energy loss is large, and the jet clustering and stability are poor. The cone nozzle [9] (figure b) has relatively uniform stress change and pressure difference distribution, but due to the lack of the stabilizing effect of the straight section, the jet is relatively diffuse and the dynamic pressure value is small. The traditional expansion nozzle (Figure c) has no cylindrical rectifying section at the outlet end, and the fluid is easy to deflect after spraying, which affects the range. Therefore, this article adds a cylindrical rectifying section at the outlet end; the expansion angle is an important factor affecting the jet effect, if the value is too large , The fluid is easy to produce wall separation, causing backflow, vortex, etc. Therefore, the expansion angle of 16º is selected in reference [10]. This nozzle has strong jet penetrating power and is suitable for high-pressure and ultra-high-pressure jets. Shrinking nozzle [11] (Figure d) The spray performance is mainly affected by the contraction angle α and the aspect ratio L/d (L: the length of the cylindrical outlet section, d: the outlet diameter). α determines the flow resistance of the nozzle, and d determines In consideration of the jet flow and smoothness, L determines the kinetic energy loss and the effect of steady flow. In this paper, the contraction angle α is 14º, length to diameter ratio is 3. The

ISSN: 2664-9640

nozzle has good jet concentration and is suitable for medium and low pressure jets. Laval nozzle [12-13] (Figure e) has the best jet effect when the contraction angle of the contraction section is 14º and the contraction section length is 2dl～6dl (dl is the diameter of the throat), and the horizontal section parameters have no influence on the jet effect. Large, the length of the expansion section is generally 6dl～8dl. The nozzle has the characteristics of low energy loss and stable performance.

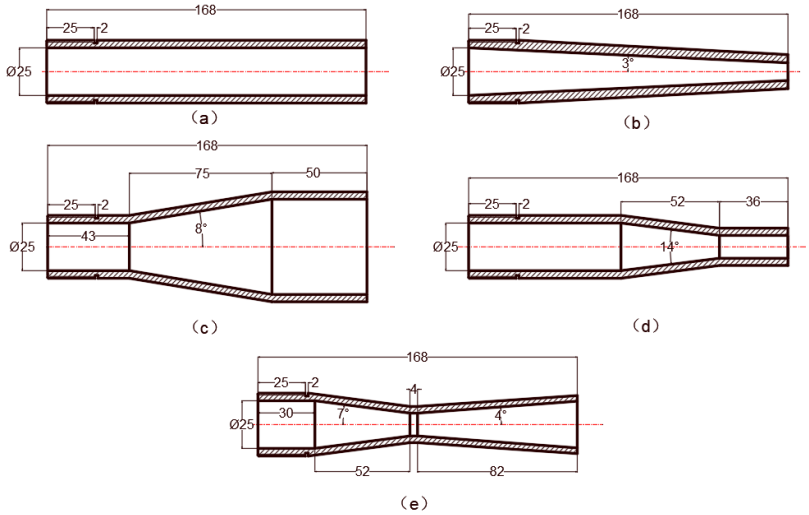

Figure.3 Nozzle model

3.2. Flow control equation

Take the straight pipe nozzle as an example to establish the two-dimensional rectangular coordinate system shown in Figure 2. Build a width of 2000 mm x 600 mm flow field, using the theory of fluid mechanics, simulation of co_2 fluid flow process inside and outside the nozzle, the flow control equations are as follows.

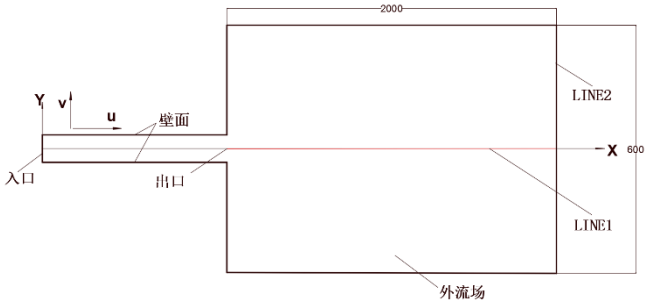

Figure.4 Flow field model outside the nozzle

Continuous equation:

$$\frac{\partial \rho}{\partial t}+\frac{\partial(\rho\mu)}{\partial x}+\frac{\partial(\rho\mu)}{\partial y}=0 \tag{9}$$

Momentum conservation equation:

X direction:

$$\frac{\partial(\rho\mu)}{\partial t}+\frac{\partial(\mu\mu)}{\partial x}+\frac{\partial(\rho\mu\upsilon)}{\partial y}=\frac{\partial}{\partial x}(\mu\frac{\partial\mu}{\partial x})+\frac{\partial}{\partial y}(\mu\frac{\partial\mu}{\partial y})-\frac{\partial p}{\partial x}+S_{\mu} \tag{10}$$

Y direction:

$$\frac{\partial(\rho\upsilon)}{\partial t}+\frac{\partial(\rho\mu)}{\partial x}+\frac{\partial(\rho\upsilon\upsilon)}{\partial y}=\frac{\partial}{\partial x}(\mu\frac{\partial\upsilon}{\partial x})+\frac{\partial}{\partial y}(\mu\frac{\partial\upsilon}{\partial y})-\frac{\partial p}{\partial y}+S\upsilon \tag{11}$$

Energy conservation equation:

ISSN: 2664-9640

$$\frac{\partial(\rho T)}{\partial t}+\frac{\partial(\rho\mu T)}{\partial x}+\frac{\partial(\rho\upsilon T)}{\partial y}=\frac{\partial}{\partial x}(\frac{k}{C_P}\frac{\partial T}{\partial x})+\frac{\partial}{\partial y}(\frac{k}{C_p}\frac{\partial T}{\partial y})+S_T \tag{12}$$

Formula: ρ is the density, t is the time, μ and υ is the component of the velocity vector at and direction at any point in the flow field X and Y, P is the pressure on the micro-element body, μ is the dynamic viscosity, S_μ and S_υ is the generalized source term, C_P is the specific heat capacity. T is the temperature, K is The heat transfer coefficient, S_T is a viscous dissipation term.

The turbulence model uses Realizable k-ε to solve the viscosity equation in a closed manner. The transport equations of k and ε in the model are:

$$\rho\frac{dk}{dt}=\frac{\partial}{\partial x_i}\left[\left(\mu+\frac{\mu_t}{\sigma_k}\right)\frac{\partial k}{\partial x_i}\right]+G_k+G_b-\rho\varepsilon-Y_M \tag{13}$$

$$\rho\frac{d\varepsilon}{dt}=\frac{\partial}{\partial x_i}\left[\left(\mu+\frac{\mu_k}{\sigma_\varepsilon}\right)\frac{\partial\varepsilon}{\partial x_i}\right]+G_{1\varepsilon}\frac{\varepsilon}{k}+(G_k+C_{3\varepsilon}G_b)-C_{2\varepsilon}\rho\frac{\varepsilon^2}{k} \tag{14}$$

Formula: G_K is the turbulent kinetic energy of an average velocity gradient; G_b is the buoyancy causing by the turbulent kinetic energy; Y_M is the compressible turbulent flow pulsation in the expansion's contribution to the total dissipation rate; the turbulent viscosity coefficient $\mu_t=\rho C_u\frac{k^2}{\varepsilon}$; $C_{1\varepsilon}=1.44$, $C_{2\varepsilon}=1.92$, $C_{3\varepsilon}=0.09$, $\sigma_k=1.0$ and respectively $\sigma_\varepsilon=1.3$ are the turbulent kinetic energy And the reciprocal of k the effective turbulent Prandtl number of the dissipation rate ε.

4. Simulation analysis of the flow field in the nozzle

4.1. Mesh division and boundary condition setting

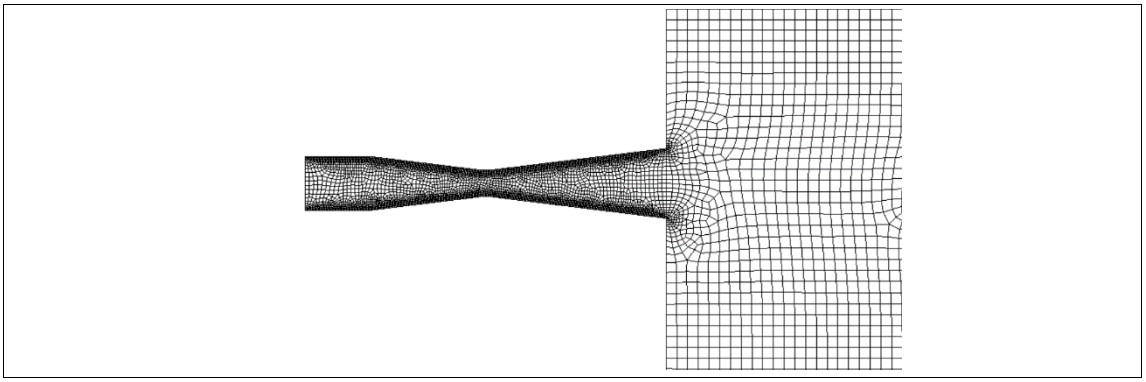

Figure.5 Grid encryption diagram of nozzle position

Symmetry between nozzle and the outflow of plant structure model. It is set as a two-dimensional plane, a quadrilateral structure is used to divide the grid, and the nozzle position is locally encrypted. Taking the Laval nozzle as an example, the grid structure diagram is shown in Figure 5. Choose the transient solver and Realizable k-ε two equation turbulence model. Using the VOF multiphase flow model, the first phase is set to liquid CO_2, the second phase is set to gaseous CO_2, and the third phase is set to air. The gas-liquid saturation line UDF is introduced into the evaporative condensation mass transfer model, and each phase state is corresponding The physical parameters are set into the material properties. Set the inlet pressure of 5 Mpa, the temperature is 285.15 K, outlet pressure of atmospheric pressure, temperature of 300K, wall surface as non-slip boundary condition, use PISO algorithm to couple pressure and velocity, define calculation step as 0.0001s, and initialize the flow field Fill up the air.

ISSN: 2664-9640

4.2. Simulation results

4.2.1. Comparative analysis of relevant data of each nozzle

In order to compare the injection situation of each nozzle, the CO_2 injection velocity and concentration in the flow field area outside the nozzle are analyzed. Two critical paths are selected according to the CO_2 injection pattern for research. Path 1 is the axis of the injection domain (line 1 in Figure 4), and path 2 is the end of the flow field (line 2 in Figure 4).

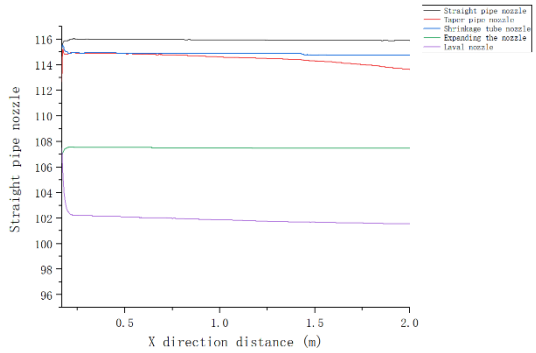

(A) LINE1 online speed comparison chart

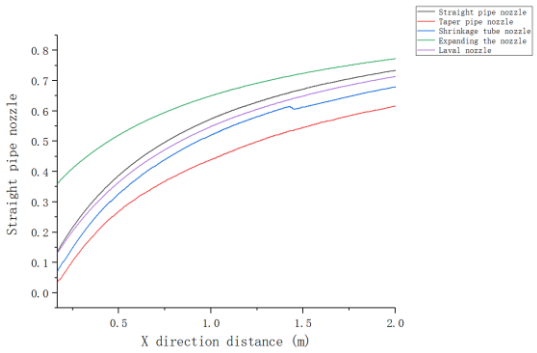

(B) Comparison chart of gaseous CO_2 volume fraction on LINE1

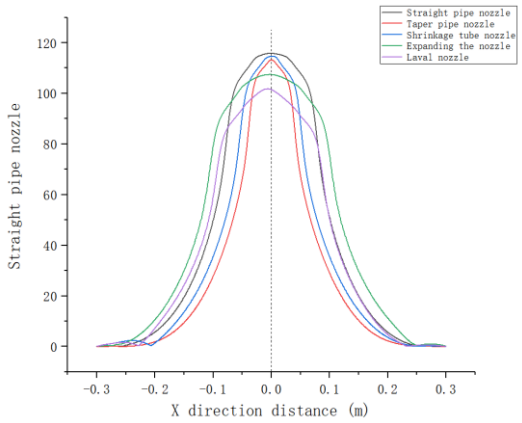

(C) LINE2 online speed comparison chart

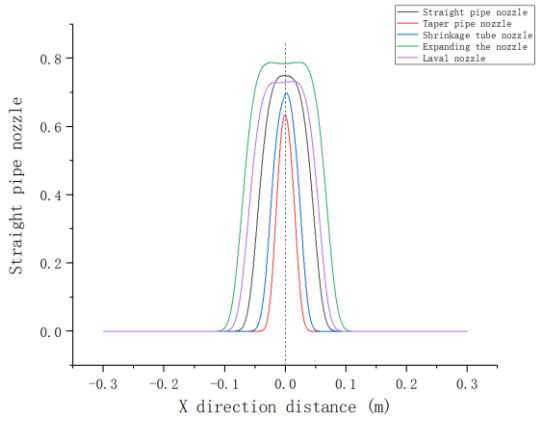

(D) Comparison chart of gaseous CO_2 volume fraction on LINE2

Figure.6 Data fitting curve diagram under two paths

From the speed comparison in Figure 6(a), it can be seen that the velocity of the fluid along the path 1 after the straight nozzle, the shrinking nozzle, and the expanding nozzle maintains 116m/s, 115m/s and 107m/s respectively; the cone nozzle is from the entrance The speed of 115m/s drops slowly to 114m/s along the path 1; the Laval nozzle drops from 108m/s at the exit to 102m/s and then slowly drops to about 101m/s along the path 1. It can be seen that, except for the Laval nozzle, the speed drop rate of the other nozzles is relatively small.

From the analysis of the CO_2 volume fraction in Figure 6(b), it can be seen that at the nozzle outlet, the gaseous CO_2 volume fraction of several nozzles gradually increases along path 1; the gaseous CO_2 volume fraction of the expanded nozzle increases along path 1 compared with the previous three nozzles Slower; the gaseous CO_2 volume fractions at the outlet of straight nozzles, tapered nozzles, shrinking nozzles, expanding nozzles, and Laval nozzles are 0.137, 0.036, 0.071, 0.361, 0.132, respectively, which shows the vaporization inside each nozzle The quantity is Expanded Nozzle>Straight Nozzle>Laval Nozzle>Reduced Pipe Nozzle>Conical Nozzle; At the end of path 1, straight pipe nozzle, tapered pipe nozzle, shrinking pipe nozzle, expanding nozzle, and Laval nozzle correspond to The gaseous volume fractions of are 0.75, 0.64, 0.70, 0.79, 0.73,

ISSN: 2664-9640

so the nozzle with the largest degree of final gasification along path 1 is the expanding nozzle, and the smallest is the cone nozzle. From the velocity analysis in Figure 6(c), it can be seen that the velocity extremes of straight nozzles, tapered nozzles, shrinking nozzles, and expanding nozzles are at the center of path 2 (ie LINE2), and the speeds are 116m/s , 113m/s, 115m/s, 107m/s, and drop symmetrically from the center point to the two ends under the interaction of air entrainment, so the jet core lines of these four nozzles are the axis lines of the flow field (That is LINE1), and the velocity extreme position of the Laval nozzle deviates from the center of path 2, so its jet core line will inevitably deviate from the axis line of the flow field, causing the jet to be inconcentrated, resulting in a large loss of kinetic energy, and its velocity extreme It is 102m/s.

From the analysis of the CO_2 volume fraction in Figure 6(d), it can be seen that the gaseous CO_2 volume coverage of several nozzles on path 2 is expanding nozzle>Laval nozzle>straight nozzle>reducing nozzle>cone nozzle. Combining figure c corresponds to the fluid velocity coverage range on path 2 respectively as expanding nozzle>Laval nozzle>straight nozzle>reducing nozzle>cone nozzle.

4.2.2. Viscosity analysis of the external flow field of each nozzle

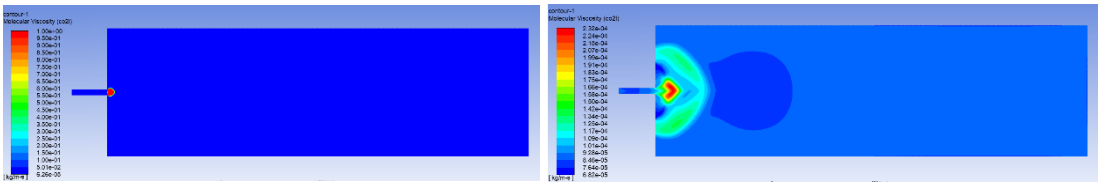

(a) 9×10^{-4}s (b) 2.3×10^{-3}s

Figure.7 Viscosity cloud diagram of the flow field outside the straight nozzle

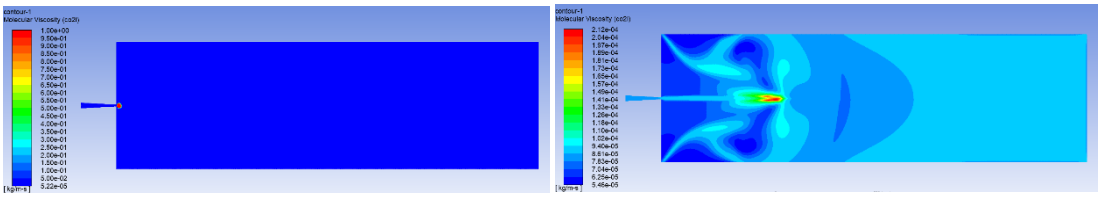

(a)1×10^{-3}s (b)1.2×10^{-2}s

Figure.8 Viscosity cloud diagram of the flow field outside the cone nozzle

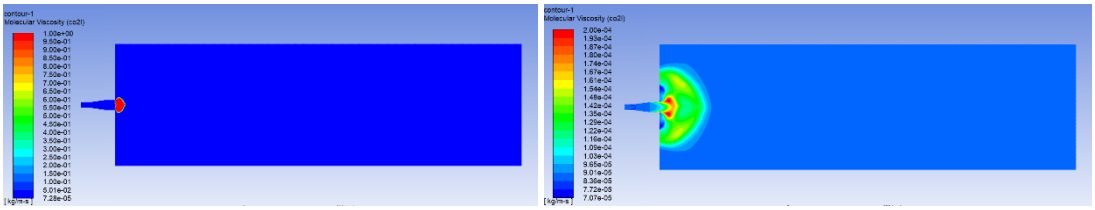

(a) 9×10^{-4}s (b) 1.9×10^{-3}s

Figure.9 Viscosity cloud diagram of the flow field outside the expanding nozzle

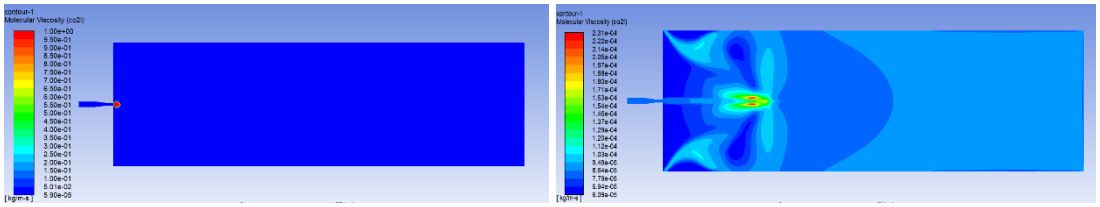

(a)9×10^{-4}s (b)1.06×10^{-2}s

Figure.10 Viscosity cloud diagram of the external flow field of the shrinking tube nozzle

ISSN: 2664-9640

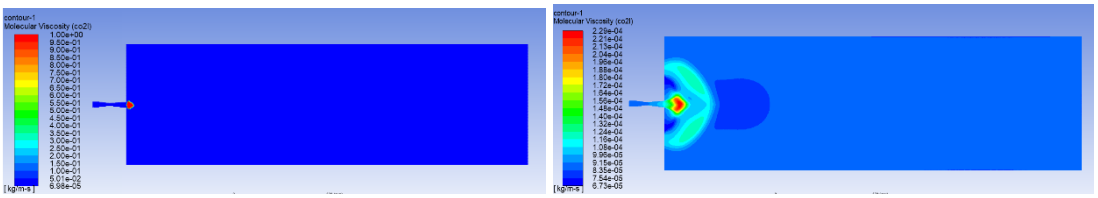

(a)1×10^{-3}s (b) 2.6×10^{-3}s

Figure.11 Viscosity cloud diagram of the flow field outside the Laval nozzle

From the above analysis of the viscosity cloud diagram of the external flow field of each nozzle, it can be seen that a certain amount of high-viscosity dry ice will be generated at the outlet of each nozzle. Under the heating of the external environment, the dry ice will continue to sublimate and dissipate along the ejection direction, and will not exceed half of the near field area. It can be seen that there is no ice blocking hazard in the nozzle, the temperature at the nozzle mouth will be very low, the sublimation rate of dry ice is very fast, and the storage range is short.

5. Conclusion

1. From the analysis of the appeal, it could be seen that the spraying speed of several nozzles is higher, all above 100m/s, so the required kinetic energy to reach the fire area could be satisfied; the degree of CO_2 gasification of the expansion nozzle was along path 1 as a whole Is the highest, reaching 75% at the end of the flow field.

2. From the comparative analysis of the data of each nozzle along path 2, it could be seen that the speed coverage and gaseous CO_2 volume fraction coverage of the expanding nozzle are both the largest, so the fire extinguishing effect would be better.

3. Dry ice would be generated at the exit of each nozzle and will continue to sublimate and dissipate along the jet direction. Dry ice could only be stored in a short time and a short distance. There was no ice blockage inside the nozzle. Therefore, dry ice could be avoided under a reasonable spray distance. The electrostatic hazard generated by the oil tank.

References

[1].Cong Dai,et al. Talking about the foam fire extinguishing system suitable for the fire extinguishing of large oil storage tank farms[J]. Science and Technology Outlook, 2016, 26(06): 158-159.

[2].Woolley R M, Fairweather M, Wareing C J,et al. Experimental measurement and reynolds-averaged navier-stokes modelling of the near-field structure of multi-phase CO2 jet releases[J].Int J Greenh Gas Con,2013,18:139-149.

[3]. Woolley R M, Fairweather M, Wareing C J, et al. An integrated, multi-scale modelling approach for the simulation of multiphase dispersion from accidental CO2, pipeline releases in realistic terrain[J]. International Journal of Greenhouse Gas Control, 2014, 27(8): 221-238.

[4]. Huh C, Cho Mi, Hong S, et al. Effect of impurities on depressurization of CO2 pipeline transport[J].Energy Procedia,2014,63:2583-2588.

[5].Witlox Hwm, Harper M, Oke A, et al. Validation of discharge and atmospheric dispersion for unpressurised and pressurised carbon dioxide releases [J]. Process Saf Environ, 2014,92: 3-16.

[6].Witlox Hwm, Harper M, Oke A, et al. Phast validation of discharge and atmospheric dispersion for pressurised carbon dioxide releases [J]. J Loss Prevent Proc,2014,30:243-255.

[7].Jamois D,Proust C and Hebrard J.Hardare and instrumentation to investigate massive releases of dense phase CO2[J].The Canadian Journal of Chemical Engineering,2015,93(2):234-240.

[8].Vree B, Ahmad M, Buit L, et al. Rapid depressurization of a CO2 pipeline-An experimental study[J]. Int JGreenh Gas Con ,2015,41:41-49.

[9]. Yi Cai, Guobing Su,et al. High-pressure water jet nozzle design and finite element analysis [J]. Mechanical Design and Research, 2017, 33(06): 163-167+171.

ISSN: 2664-9640

[10].Jie Xu,Bingqian Li, Jian Li,Et al.The structure design of a shrinking jet tube[J]. Machine Tool and Hydraulics, 2017, 45(02): 119-122.

[11].Shengmin Pang, Peimin Chen,et al. Design of cylindrical nozzle based on CFD[J]. Machinery Manufacturing and Automation, 2011, 40(01): 41-42+89.

[12].Qingwei Feng,et al. Design and experimental research of steam jet nozzle[J]. Petroleum Field Machinery, 2015, 44(06): 43-46.

[13].Zhaoqiang Sun, Xing Zhang, Baoyu Liu, et al. Optimization design of jet cleaner nozzle based on numerical simulation of flow field[J]. Oil & Gas Storage and Transportation, 2020, 39(02): 201-208.